IOPscience iopscience.iop.org

Home Search Collections Journals About Contact us My IOPscience

An embedding approach to electron waveguides

This article has been downloaded from IOPscience. Please scroll down to see the full text article.

1998 J. Phys.: Condens. Matter 10 5923

(http://iopscience.iop.org/0953-8984/10/26/018)

View the table of contents for this issue, or go to the journal homepage for more

Download details:
IP Address: 171.66.16.209
The article was downloaded on 14/05/2010 at 16:34

Please note that terms and conditions apply.

J. Phys.: Condens. Matter **10** (1998) 5923–5941. Printed in the UK PII: S0953-8984(98)92656-X

An embedding approach to electron waveguides

Elizabeth Dix and John E Inglesfield

Department of Physics and Astronomy, University of Wales, Cardiff, PO Box 913, Cardiff CF2 3YB, UK

Received 20 March 1998

Abstract. A new and flexible method has been developed for studying the transport properties of electron waveguides. The approach uses the embedding method for confined quantum systems to calculate the eigenstates and Green function for the structures. The infinite potential at the waveguide walls is replaced by an embedding potential which is added onto the Hamiltonian for the inside of the waveguide. The wavefunction or Green function is then expanded in any convenient basis set and the transmission and reflection coefficients calculated. In this paper we have studied a 90° circular corner, a right-angled corner and a kink. To understand the transmission results more fully the current density has been calculated. Bound states and resonances have also been explored for the two corner geometries by calculating the local density of states. Both the transmission and local density of states exhibit lineshapes which correspond to scattering Fano resonances.

1. Introduction

There is much interest in the transport properties of electrons in mesoscopic structures, due on the one hand to advances in fabrication technology, and on the other hand to theoretical developments in quantum conductance [1]. The size of these structures, on the scale of nanometres, is comparable with the carrier elastic and inelastic mean free paths, and the transport is ballistic with scattering at the boundaries dominating. In this paper we describe a new and flexible method for calculating the transport properties of mesoscopic structures, using the embedding method [2] for calculating the electron Green function. The method can be used for any mesoscopic structure, but here we concentrate on the transport properties of electron waveguides. These waveguides are used as connections between devices, and it is therefore inevitable, due to size constraints, that they will be curved. In this paper we compare the transport properties of a 90° circular corner, a right-angled corner and a kink (figure 1); we shall use the current densities to show how electrons go round corners, and in particular how electrons can become trapped.

Our model of the waveguide is standard—a constant potential bounded by reflecting walls. In our method, the infinite potential at the walls is replaced by an embedding potential which is added onto the Hamiltonian for the inside of the waveguide. Any convenient basis set can be used to expand the electron wavefunctions or Green functions, and the embedding potential imposes the right boundary conditions of reflection at the boundary. The advantages of this embedding method are firstly, that it is flexible, easy to set up, and computationally efficient; secondly, that the embedding potential can be chosen either to describe hard boundary conditions (specular reflection) or softer boundary conditions to describe loss processes; and thirdly, that the use of basis functions makes it easy to include atomic potentials or external fields.

0953-8984/98/265923+19$19.50 © 1998 IOP Publishing Ltd

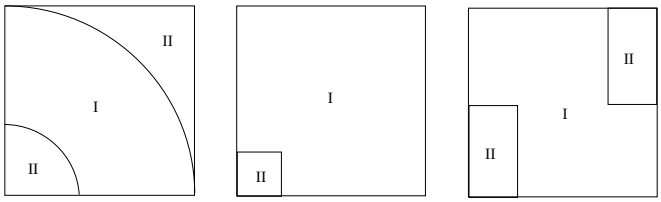

Figure 1. A schematic diagram of the corner geometries studied.

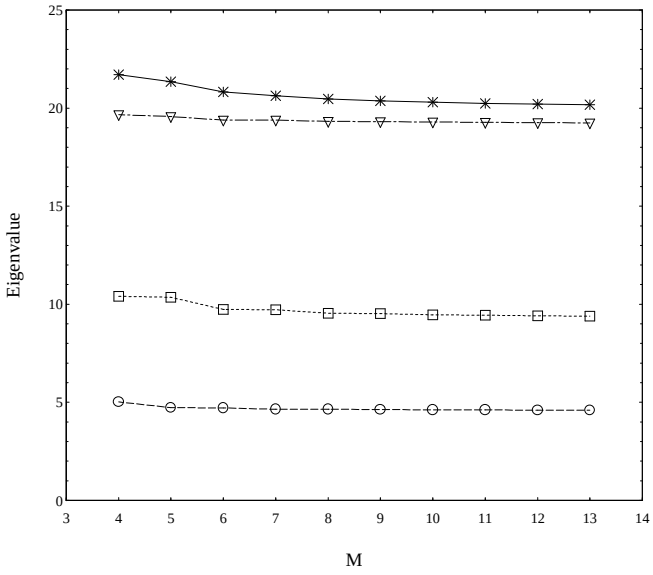

Figure 2. The convergence of the first four eigenvalues with M (where M^2 is the basis set size), for the circular corner, with inner radius 0.2 au and outer radius 1.2 au.

Previous studies on curved waveguides can be divided into two main groups. The first of these involves mode matching [3–6], in which the guide is divided into three separate regions: the input and output leads, and the corner region. Solutions of the Schrödinger equation at a particular energy are then matched in amplitude and derivative at the interfaces of the three regions. This method has been applied by Sols and Macucci [3], for example, to study transmission through circular corners. Explicit forms for the wavefunction in the straight input and output leads and the circular corner itself are used, with Schrödinger's equation in the corner region being expressed in polar coordinates. In the second class of methods, the Schrödinger equation is discretized in the region of the waveguide bend, and the wavefunction calculated numerically [7]. An efficient method of calculating the Green function for a discretized Hamiltonian is the 'causal-surface Green's function method' of Pendry *et al* [8], which they have applied to calculations of ballistic electron transport in waveguides with complex geometry. More complicated structures can be divided up into slices, for each of which the transmission and reflection matrices are found [9].

The plan of this paper is as follows. The embedding method for calculating the electron Green function in waveguides is described in section 2, and the calculation of reflection and transmission coefficients and current density in section 3. The results for the different waveguide geometries are presented in section 4, and compared with previously published

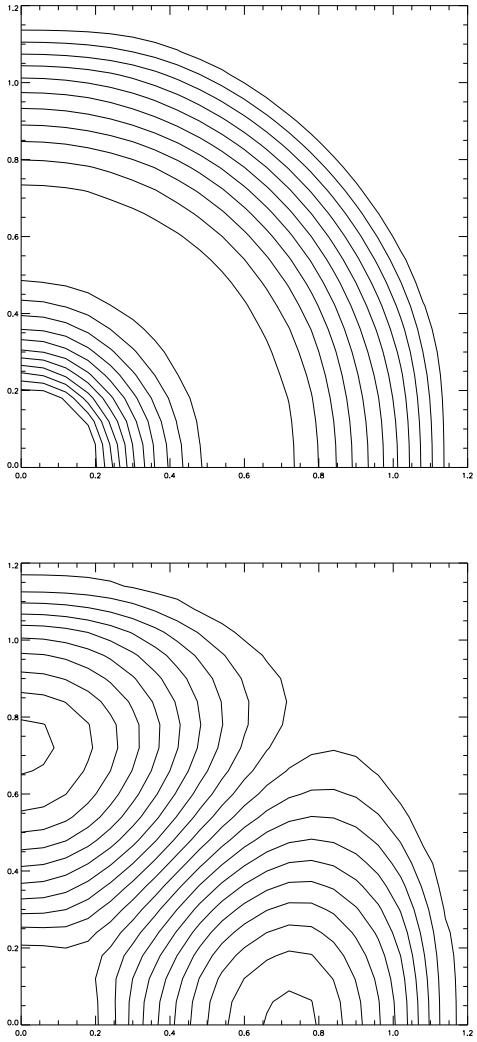

Figure 3. Wavefunctions for the first two eigenvalues for the circular corner.

calculations. Finally in section 5, bound-state energies and local densities of states for the two corners are presented.

We use atomic units, with $e = \hbar = m = 1$, throughout.

2. Embedding for confined systems

Embedding is a convenient way of solving the Schrödinger equation in a region of space I, joined over surface S onto some substrate region II. The wavefunction has to match in amplitude and derivative across S, which is equivalent to solving the Schrödinger equation in I subject to the boundary condition that the wavefunction has the right logarithmic derivative. The embedding method gives a way of specifying this boundary condition, and

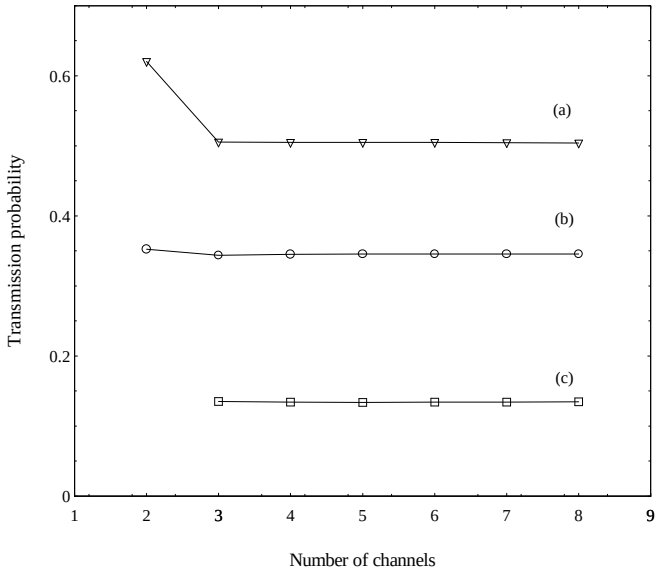

Figure 4. The convergence of the partial transmission probabilities, T_{pq}, with the number of channels. Plot (a) is the probability for an electron in channel 1 to be transmitted into channel 1, (b) is that for transmission into channel 2 from channel 1 and (c) is that for transmission into channel 3 from channel 1.

it results in the following variational principle for a trial function defined only in region I:

$$E = \left[\int_I \mathrm{d}^3 r\ \phi H\phi + \frac{1}{2}\int_S \mathrm{d}^2 r_s\ \phi\frac{\partial\phi}{\partial n_s} + \int_S \mathrm{d}^2 r_s \int_S \mathrm{d}^2 r_s'\ \phi\left(G_0^{-1} - \epsilon\phi\frac{\partial G_0^{-1}}{\partial\epsilon}\right)\phi\right] \times \left[\int_I \mathrm{d}^3 r\ \phi^2 - \int_S \mathrm{d}^2 r_s \int_S \mathrm{d}^2 r_s'\ \phi\frac{\partial G_0^{-1}}{\partial\epsilon}\phi\right]^{-1}. \tag{1}$$

Here $\partial\phi/\partial n_s$ is the outward-normal derivative of ϕ on S; G_0^{-1}, the embedding potential, is the surface inverse of G_0, the Green's function for region II evaluated at some energy ϵ with zero normal derivative on S. The energy derivative of G_0^{-1}, which appears in both the numerator and denominator, provides a correction to the embedding potential so that it is evaluated (to first order) at energy E rather than ϵ.

Minimizing E, ϕ satisfies the Schrödinger equation

$$H\phi = E\phi \tag{2}$$

inside region I, and at the boundary ϕ and $\partial\phi/\partial n_s$ match correctly onto the solution of the Schrödinger equation in region II.

In the case of electrons confined by an infinite barrier potential, the confinement region constitutes region I, and the infinite potential is replaced by a very large constant potential V, constituting region II. The embedding potential which replaces region II is then given by

$$G_0^{-1}(\boldsymbol{r}_s, \boldsymbol{r}_s') \approx \sqrt{\frac{V}{2}}\delta(\boldsymbol{r}_s - \boldsymbol{r}_s'). \tag{3}$$

For large V it is a local potential, and energy independent, and hence (1) simplifies.

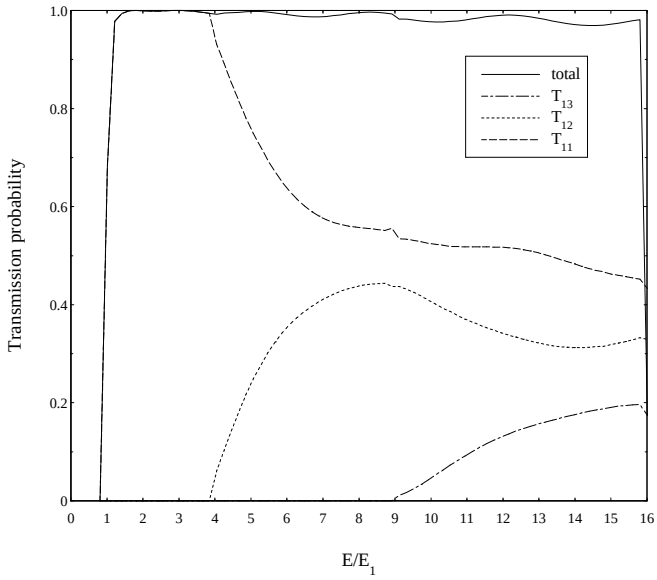

Figure 5. The transmission probabilities T_{pq} as functions of the energy relative to the first threshold energy, for input into channel 1, for the circular corner.

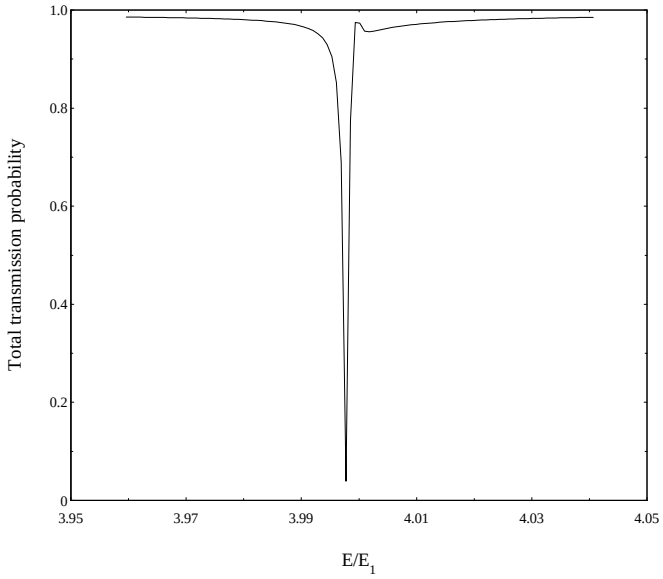

Figure 6. The total transmission as a function of the energy for the energy window near the first threshold energy for the circular corner, demonstrating the rapid change in transmission.

Minimizing E then leads to a wavefunction satisfying (2), and at the boundary

$$\frac{\partial \phi(\boldsymbol{r}_s)}{\partial n_s} = -\sqrt{2V}\phi(\boldsymbol{r}_s). \tag{4}$$

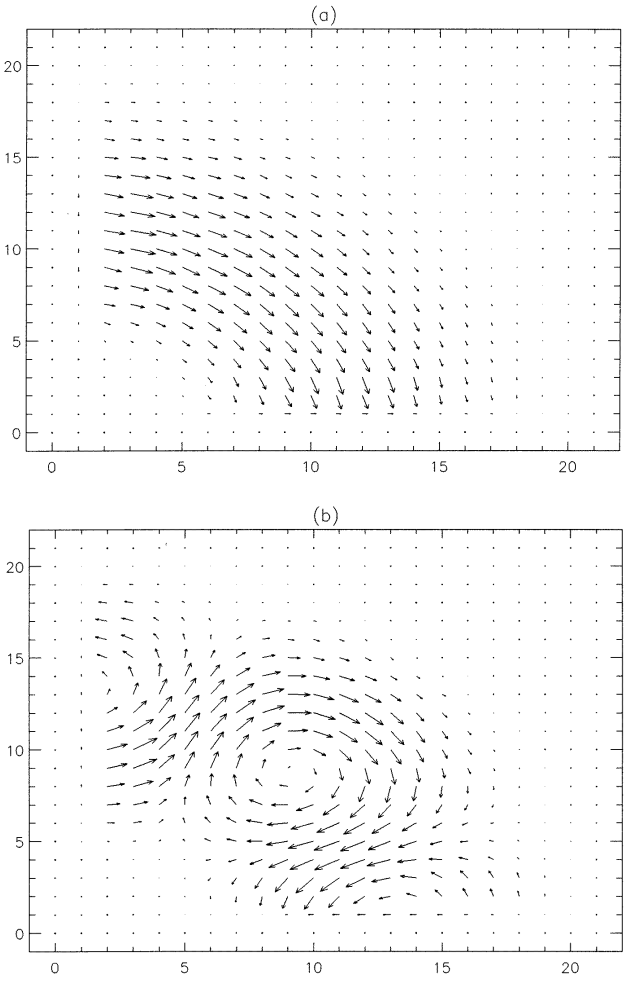

Figure 7. The current density for the circular corner at (a) $E = 6.0$ ($1.2 \times E_1$), (b) $E = 19.71$ ($3.995 \times E_1$), (c) $E = 19.73$ ($3.998 \times E_1$), (d) $E = 19.74$ ($3.999 \times E_1$).

For large V, and well-behaved functions, this means that

$$\phi(\boldsymbol{r}_s) \approx 0 \tag{5}$$

as we require. In practice, very large values of V can be used, typically 10^5 au, and exponential decay of the wavefunction into II can be made as small as we like.

To find the eigenstates, ϕ is expanded in terms of basis functions χ_i, not satisfying any particular boundary conditions on S:

$$\phi(\boldsymbol{r}) = \sum_i a_i \chi_i(\boldsymbol{r}). \tag{6}$$

Then the variational principle gives the generalized eigenvalue equation:

$$\sum_j H_{ij} a_j = E \sum_j O_{ij} a_j \tag{7}$$

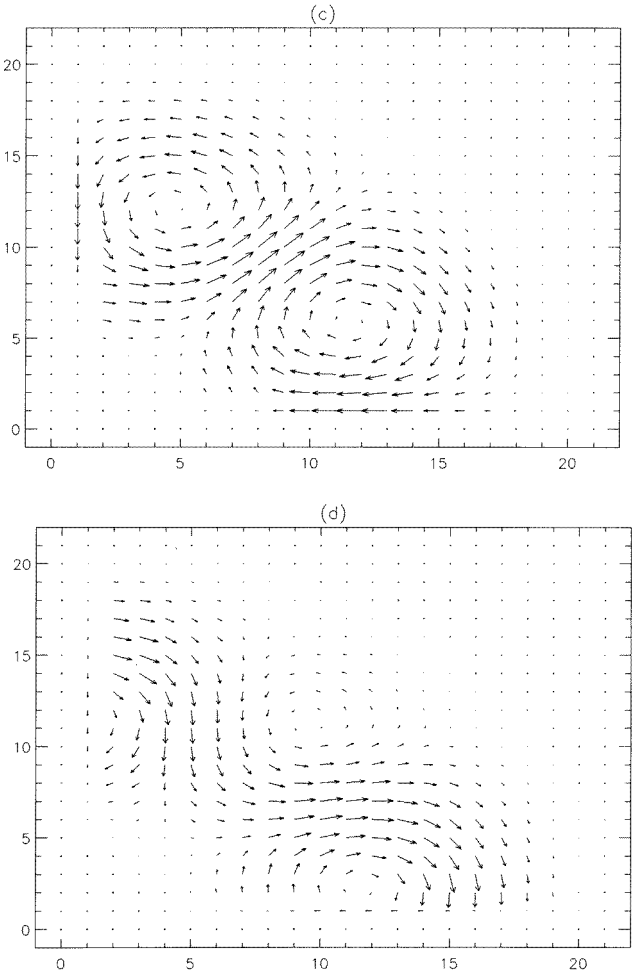

Figure 7. (Continued)

with the following matrix elements:

$$H_{ij} = \int_I \mathrm{d}^3 r\ \chi_i(\boldsymbol{r}) H \chi_j(\boldsymbol{r}) + \frac{1}{2}\int_S \mathrm{d}^2 r_s\ \chi_i \frac{\partial \chi_j}{\partial n_s} + \sqrt{\frac{V}{2}}\int_S \mathrm{d}^2 r_s\ \chi_i(\boldsymbol{r}_s)\chi_j(\boldsymbol{r}_s)$$
$$O_{ij} = \int_I \mathrm{d}^3 r\ \chi_i(\boldsymbol{r})\chi_j(\boldsymbol{r}). \tag{8}$$

The Green's function for this confined system, satisfying

$$\left(-\frac{1}{2}\nabla^2 + V - E\right) G(\boldsymbol{r}, \boldsymbol{r}') = \delta(\boldsymbol{r} - \boldsymbol{r}') \qquad \boldsymbol{r}, \boldsymbol{r}' \text{ in I} \tag{9}$$

with

$$G(\boldsymbol{r}_s, \boldsymbol{r}') \approx 0$$

is given by

$$G(\boldsymbol{r}, \boldsymbol{r}') = \sum_{ij} (H - EO)^{-1}_{ij} \chi_i(\boldsymbol{r})\chi_j(\boldsymbol{r}') \tag{10}$$

and we shall use this in section 3 to calculate the transmission coefficients of the waveguide.

As an example of the embedding method, we shall calculate the wavefunctions for the circular corner shown in figure 1. The wavefunctions should go to zero at the edges of the waveguide, and we shall also impose a zero-derivative boundary condition at the ends of the piece of waveguide. (This zero-derivative boundary condition is needed subsequently, as we shall see in section 3, for calculating the transmission.) The basis functions that we use are

$$\chi_i = \cos\frac{k\pi x}{r_2}\cos\frac{l\pi y}{r_2} \tag{11}$$

where r_2 is the square side—the outer radius; these automatically satisfy the zero-derivative boundary condition at the ends, but do not satisfy any conditions on the sides of the waveguide. Figure 2 shows the convergence of the first four eigenvalues with basis set size for a circular corner with inner and outer radii 0.2 and 1.2 au. The embedding potential that we use corresponds to a confining potential of 10^5 au. The eigenvalues converge well, with a basis set size of 11×11 giving very accurate eigenvalues. Typical results for the wavefunctions are shown in figure 3, and we see that they go nicely to zero at the waveguide boundary.

The advantages of the embedding method are well demonstrated by this example—flexibility in the choice of basis function, and excellent, uniform convergence. With this plane-wave basis set, it would also be very easy to calculate the transmission through the impurity atoms in region I, for example [10, 11]. The reason for the good convergence is that the system is unconstrained outside region I. If the basis set is too big, problems of overcompleteness can arise, but these can be minimized by increasing the numerical accuracy, and seem to be rarely problematic.

3. Transmission, reflection and current density

To calculate the transmission and reflection coefficients of region I, we use the Green function to find the transmitted and reflected wavefunctions originating from a particular incident wave. Let us write the total wavefunction due to this incident wave as ψ; then in region I inside the waveguide, ψ and G satisfy the Schrödinger equation:

$$\left(-\frac{1}{2}\nabla^2 + V(\boldsymbol{r}) - E\right)\psi(\boldsymbol{r}) = 0 \tag{12}$$

$$\left(-\frac{1}{2}\nabla^2 + V(\boldsymbol{r}) - E\right)G(\boldsymbol{r},\boldsymbol{r}') = \delta(\boldsymbol{r},\boldsymbol{r}'). \tag{13}$$

Multiplying equation (12) by G, equation (13) by ψ, subtracting, and integrating through I gives

$$\psi(\boldsymbol{r}') = \frac{1}{2}\int_I \mathrm{d}^3\boldsymbol{r}' \left[G(\boldsymbol{r},\boldsymbol{r}')\,\nabla^2\psi(\boldsymbol{r}) - \psi(\boldsymbol{r})\,\nabla^2 G(\boldsymbol{r},\boldsymbol{r}')\right]. \tag{14}$$

Using Green's theorem this becomes

$$\begin{aligned}\psi(\boldsymbol{r}') = {} & \frac{1}{2}\int_{RH} \mathrm{d}^2\boldsymbol{r}_s \left[G(\boldsymbol{r}',\boldsymbol{r}_s)\frac{\partial\psi(\boldsymbol{r}_s)}{\partial n_s} - \psi(\boldsymbol{r}_s)\frac{\partial G(\boldsymbol{r}',\boldsymbol{r}_s)}{\partial n_s}\right] \\ & - \frac{1}{2}\int_{LH} \mathrm{d}^2\boldsymbol{r}_s \left[G(\boldsymbol{r}',\boldsymbol{r}_s)\frac{\partial\psi(\boldsymbol{r}_s)}{\partial n_s} - \psi(\boldsymbol{r}_s)\frac{\partial G(\boldsymbol{r}',\boldsymbol{r}_s)}{\partial n_s}\right]\end{aligned} \tag{15}$$

where the surface integrals are over the right-hand and left-hand ends of the waveguide, and the normal derivatives are taken from left to right along the waveguide—outside to inside

at the left-hand end and inside to outside for the right-hand end. This equation simplifies if we take G to satisfy zero-derivative boundary conditions at both ends, and putting $\boldsymbol{r}'$ at each end we obtain the integral equations

$$\psi_{LH} = \frac{1}{2}\int_{RH} \mathrm{d}^2\boldsymbol{r}'_R \; G(\boldsymbol{r}_L, \boldsymbol{r}'_R)\frac{\partial\psi(\boldsymbol{r}'_R)}{\partial n_s} - \frac{1}{2}\int_{LH} \mathrm{d}^2\boldsymbol{r}'_L \; G(\boldsymbol{r}_L, \boldsymbol{r}'_L)\frac{\partial\psi(\boldsymbol{r}'_L)}{\partial n_s} \tag{16}$$

$$\psi_{RH} = \frac{1}{2}\int_{RH} \mathrm{d}^2\boldsymbol{r}'_R \; G(\boldsymbol{r}_R, \boldsymbol{r}'_R)\frac{\partial\psi(\boldsymbol{r}'_R)}{\partial n_s} - \frac{1}{2}\int_{LH} \mathrm{d}^2\boldsymbol{r}'_L \; G(\boldsymbol{r}_R, \boldsymbol{r}'_L)\frac{\partial\psi(\boldsymbol{r}'_L)}{\partial n_s} \tag{17}$$

where $\boldsymbol{r}_L$ and $\boldsymbol{r}_R$ are now the surface variables over the left-hand and right-hand ends of region I.

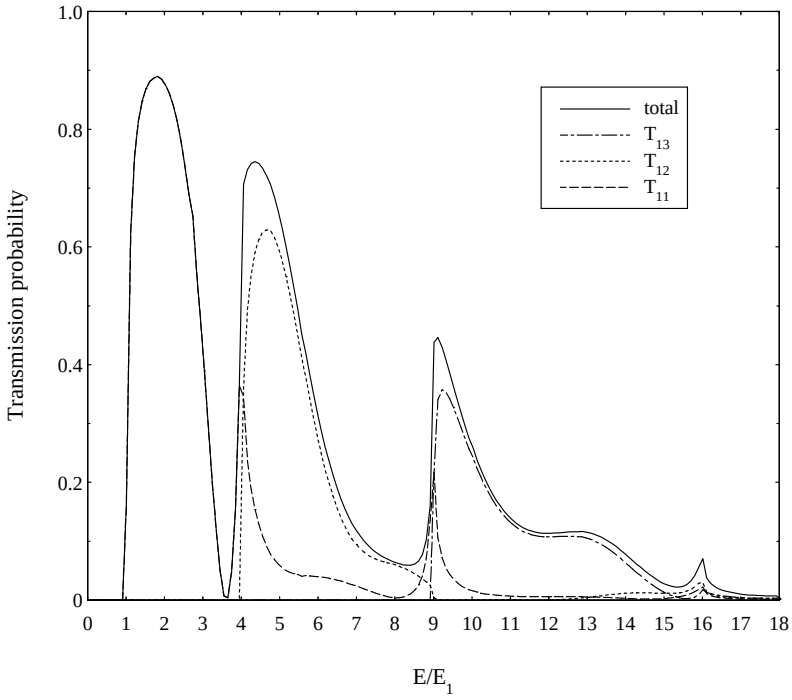

Figure 8. The transmission probabilities T_{pq} as functions of the energy (relative to the first threshold energy) for the square corner.

In the straight input and output waveguides connected to region I, the wavefunction at energy E is a linear combination of channel functions:

$$\psi_p^{\pm}(x, y) = \sin\left(\frac{p\pi y}{w}\right)\exp(\pm \mathrm{i}k_p x) \tag{18}$$

$$k_p^2 = 2E - \frac{p^2\pi^2}{w^2}. \tag{19}$$

w is the width of the guide, with variable y along the width and x along the length (confinement in the z-direction just adds a constant energy to the whole problem). Then the total wavefunction in the input waveguide connected to the left-hand end of region I, corresponding to an incident wave in channel q, is given by

$$\psi = \sum_p (\delta_{pq}\exp(\mathrm{i}k_p x) + r_{pq}\exp(-\mathrm{i}k_p x))\sin\left(\frac{p\pi y}{w}\right) \tag{20}$$

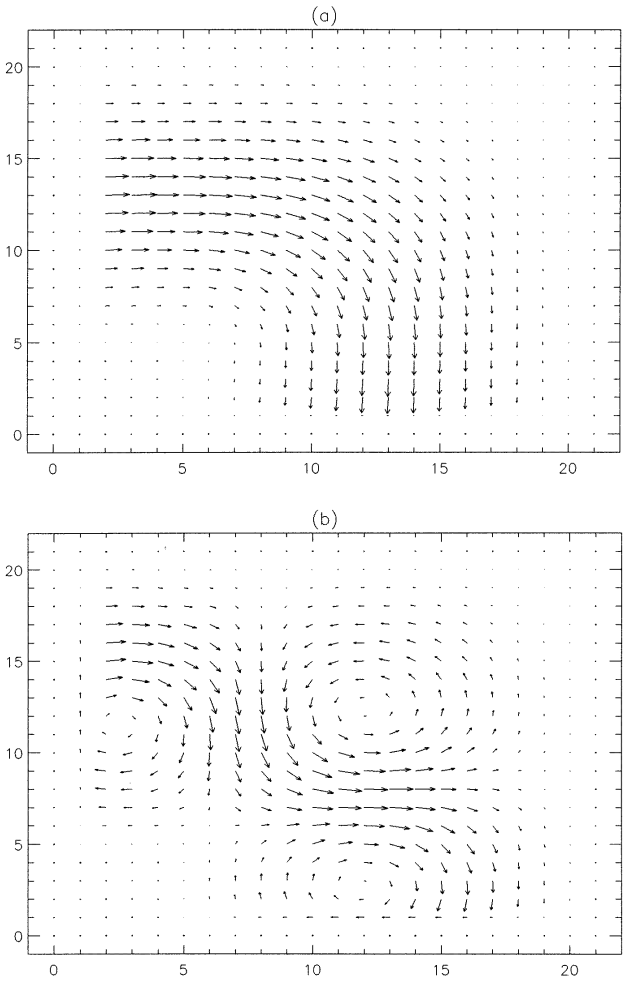

Figure 9. The current density for the square corner at (a) $E = 9.87$ $(2 \times E_1)$, (b) $E = 18.8$ $(3.8 \times E_1)$, (c) $E = 24.7$ $(5 \times E_1)$, (d) $E = 39.5$ $(8 \times E_1)$.

and in the output waveguide connected to the right-hand end

$$\psi = \sum_p t_{pq} \exp(\mathrm{i}k_p x) \sin\left(\frac{p\pi y}{w}\right). \tag{21}$$

We note that q is always an open channel—one for which k_q in (19) is real—whereas p is summed over all channels, including those for which k_p is imaginary.

To find the reflection and transmission coefficients r_{pq} and t_{pq}, we substitute (20) and (21) into (16) and (17). At the left-hand end we have

$$\begin{aligned} \psi(\boldsymbol{r}_L) &= \sum_p (\delta_{pq} + r_{pq}) \sin\left(\frac{p\pi y}{w}\right) \\ \frac{\partial \psi(\boldsymbol{r}_L)}{\partial n_s} &= \sum_p (\delta_{pq} - r_{pq}) \mathrm{i}k_p \sin\left(\frac{p\pi y}{w}\right) \end{aligned} \tag{22}$$

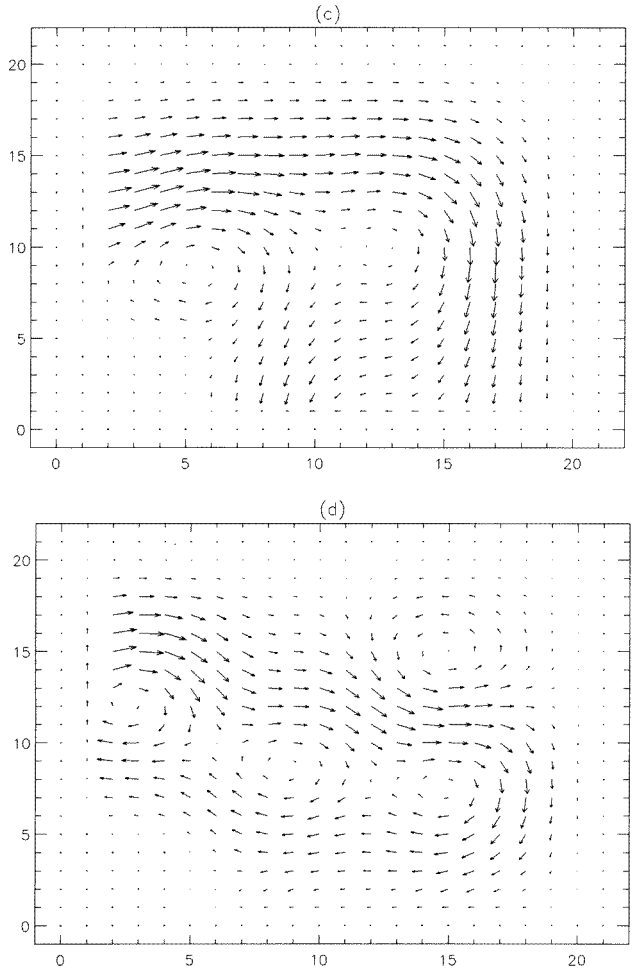

Figure 9. (Continued)

and at the right-hand end

$$\psi(\boldsymbol{r}_R) = \sum_p t_{pq} \sin\left(\frac{p\pi y}{w}\right)$$
$$\frac{\partial\psi(\boldsymbol{r}_R)}{\partial n_s} = \sum_p \mathrm{i}k_p t_{pq} \sin\left(\frac{p\pi y}{w}\right) \tag{23}$$

Substituting into (16) and (17), the integral equations become matrix equations for r_{pq} and t_{pq}; the sum over channels has to be truncated, of course, and in practice six channels are sufficient for q in the first three open channels. What is relevant for conductance is

$$T_{pq} = |t_{pq}|^2 \frac{v_p}{v_q} \tag{24}$$

$$R_{pq} = |r_{pq}|^2 \frac{v_p}{v_q} \tag{25}$$

where v_p and v_q are the wave velocities in the channels, so T_{pq} and R_{pq} represent the

transmission and reflection probabilities respectively. To understand our transmission results we shall also calculate the current density. This is given by

$$\boldsymbol{J} = \frac{1}{2\mathrm{i}}\left(\psi^* \boldsymbol{\nabla}\psi - \psi \boldsymbol{\nabla}\psi^*\right) \tag{26}$$

Having found r_{pq}, t_{pq} and consequently knowing $\psi(\boldsymbol{r}_L)$, $\partial\psi(\boldsymbol{r}_L)/\partial n_s$ etc we can find $\psi(\boldsymbol{r})$, and hence $\boldsymbol{J}(\boldsymbol{r})$ throughout region I from our Green function result (15). Current flow studies have also been done by Ji [12], Berggren *et al* [6, 13] and Lent [14], who have examined double circular bends, a cross-bar structure and a cavity in a quantum waveguide.

4. Transmission round corners

To begin with, we shall examine the convergence of the transmission probabilities for the circular corner using the same system which we used to check the convergence of the eigenvalues in section 2. It was found from the eigenvalue convergence that a basis set size of 11×11 gave an accurate value, and we thus use this size for the rest of the calculations. Figure 4 shows how the transmission probabilities converge as the number of channels is increased, at a fixed energy of 12 relative to the threshold energy for the first channel. The transmission probabilities converge well, and six channels are sufficient to give an accurate value.

We now go on to look at the energy dependence of the transmission round the circular corner. Figure 5 shows the partial transmission probabilities for input in channel 1 as functions of the energy (relative to the threshold energy for this channel). The results are identical to those of Sols and Macucci [3] and Lent [7]. As the energy increases, the higher-order exit channels open up and it is then possible for the incoming wave incident in the first channel to be scattered into one of these higher-order channels. Although not apparent on the energy scale of figure 5, the transmission at energies just below the channel threshold energies changes rapidly. This can be seen in figure 6 where we have zoomed in on the region around the first threshold energy, and we see that the transmission drops to zero very sharply and rises just as rapidly. This lineshape corresponds to a scattering Fano resonance in which the continuum of the first channel interacts with a bound state just below the threshold in the second channel [15]. Interference between direct transmission in the first channel and transmission via the bound state in the second channel leads to this lineshape. In section 5 we shall examine the Fano resonances further. The total transmission probability is practically unity at all energies except in these tiny energy windows just below the threshold energies, showing that the corner does not seriously restrict the flow of electrons.

Next we will look at the current density in the circular corner. This has been evaluated using equation (26), and is shown in figure 7. Here it is plotted for particular energies using arrows which represent the direction and magnitude of the current density over a grid of points in the guide. As the energy increases and more exit channels open up, the current density goes from a laminar flow pattern to one which is more complicated. Particularly interesting is the current density within the small energy window just below the first threshold energy; here the flow pattern changes rapidly from a uniform flow pattern to one which contains current vortices. This can be seen in figures 7(b), 7(c) and 7(d) where the current density has been plotted for energies just above, just below and at the first dip in the transmission. When the transmission is a minimum (figure 7(c)) the electrons get trapped in the corner and circulate round these vortices. Despite the complicated current flow, the total transmission is practically unity everywhere except at the anti-resonances close to the thresholds.

We now consider the right-angled corner. We use the same width of waveguide and confining potential that we used for the circular corner. The transmission probabilities as functions of the energy can be seen in figure 8, once again for input in channel 1. The transmission results are the same as those published by Wu *et al* [5] and Weisshaar *et al* [16]. First we look at the total transmission probability shown in figure 8. Unlike the case for the circular corner, the total transmission probability is always less than unity and has larger energy windows in which the transmission drops to near zero. As before, these abrupt changes occur near the threshold energies for a new channel. It can be seen from the partial transmission probabilities, shown in figure 8, that as the energy increases and a new channel opens up, the new channel carries most of the current until the next threshold is reached. In other words the square corner behaves as quite an efficient mode convertor. The current-density plots (figure 9) give some idea about what is happening to the electrons at these energies. They have been plotted for energies at which maximum and minimum transmission occurs. It can be seen that at a minimum in transmission, as with the circular corner, the electrons get trapped in the corner and travel round the vortices with little transmission. As before, the current density starts with laminar flow and acquires more structure as the energy increases.

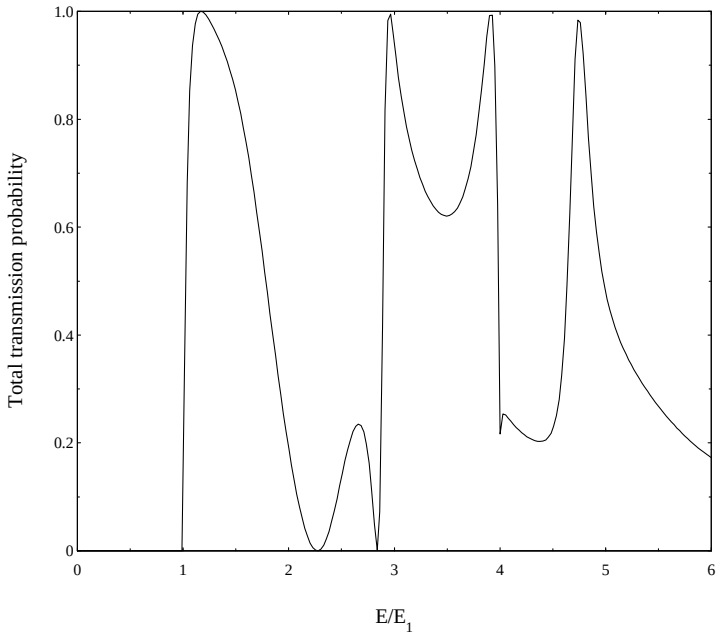

Figure 10. The total transmission probability as a function of the energy for the kink.

Finally, we shall discuss the results for the kink. The results shown are for a kink with width 0.5 au and length 1.0 au (figure 1). Figure 10 shows the total transmission probability as a function of the energy, which is almost identical to the results published by Yalabik [17]. There is more structure in this transmission curve than for the other corners, again with peaks and troughs corresponding to energies at which a new channel opens up. As with the square corner, the total transmission drops to zero at some points. From the current-density plots (figure 11) it can be seen that at the energy of the first minimum (figure 11(b)) there is total reflection at the edges and the electron is trapped inside the corner and circulates

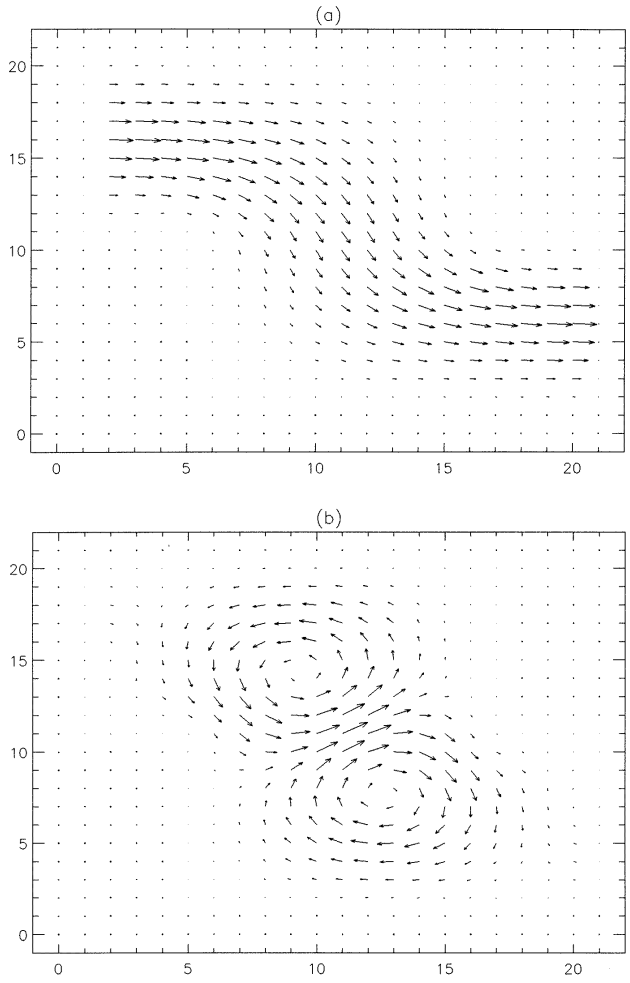

Figure 11. The current density for the kink at (a) $E = 23.0$ $(1.17 \times E_1)$, (b) $E = 45.0$ $(2.28 \times E_1)$, (c) $E = 59.0$ $(2.99 \times E_1)$ and (d) $E = 94.0$ $(4.76 \times E_1)$.

round without transmission. Again the current flow pattern becomes more complicated as the energy is increased and more exit channels open up.

5. Bound states and resonances

We shall now calculate the density of states of the corners, in order to study bound states [18] and resonances—from general scattering theory, resonances will affect the transmission [19]. The density of states—a static property of the system—has hardly been looked at till now, though Ulreich and Zwerger [20] have recently published results for a quantum point contact. It can be conveniently calculated in our approach, by adding embedding potentials to the left- and right-hand ends of region I to simulate—exactly—the effect of matching the states in the corner region onto the wavefunctions in the connecting waveguides.

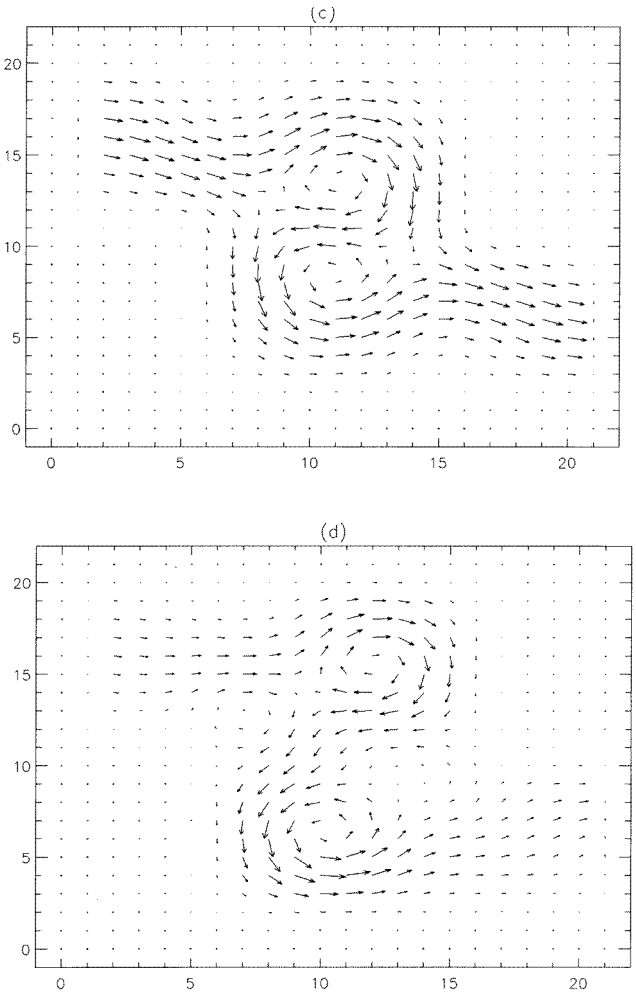

Figure 11. (Continued)

The embedding potential, Σ, can be found directly from the formula

$$-\frac{1}{2}\frac{\partial\psi(\boldsymbol{r}_s)}{\partial n_s} = \int_S \mathrm{d}^2\boldsymbol{r}_s'\ \Sigma(\boldsymbol{r}_s, \boldsymbol{r}_s')\psi(\boldsymbol{r}_s'). \tag{27}$$

This is a generalized logarithmic derivation giving the derivative of the states at the junction of the straight waveguide in terms of the amplitude. The integral in (27) is over this boundary, and the normal derivative is outwards from the corner region. As we are interested in the static density of states, the embedding potentials correspond to outgoing travelling waves from region I in open channels, and outwardly decaying exponentials in the closed channels. In the left-hand waveguide the solutions of Schrödinger's equation at energy E are then given by

$$\psi_p(x, y) = \sin\left(\frac{p\pi y}{w}\right)\exp(-\mathrm{i}kx) \tag{28}$$

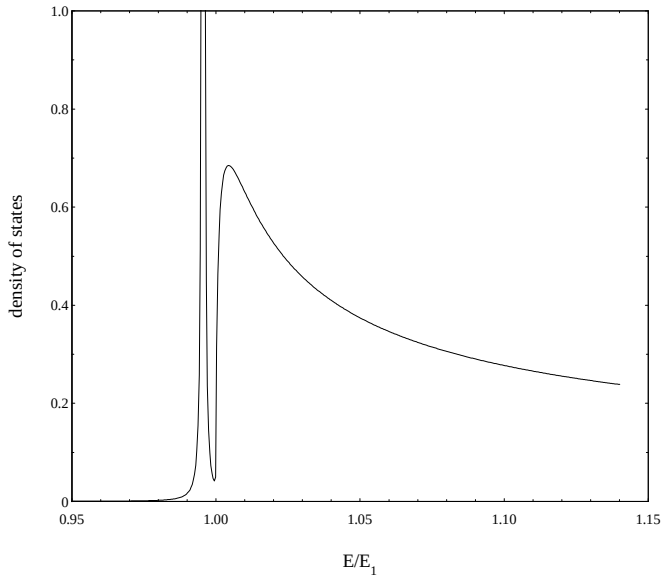

Figure 12. The density of states as a function of the energy (relative to the first threshold energy) near the bound-state energy for the circular corner.

where

$$k^2 = 2E - \frac{p^2\pi^2}{w^2}$$

if positive, or

$$\psi_p(x, y) = \sin\left(\frac{p\pi y}{w}\right)\exp(\gamma x) \tag{29}$$

where

$$\gamma^2 = \frac{p^2\pi^2}{w^2} - 2E$$

if negative.

From these we can obtain the outward-normal derivatives:

$$\frac{\partial\psi_p}{\partial n_s} = -\frac{\partial\psi_p}{\partial x} = \mathrm{i}k\sin\left(\frac{p\pi y}{w}\right)\exp(-\mathrm{i}kx) \tag{30a}$$

or

$$\frac{\partial\psi_p}{\partial n_s} = -\gamma\sin\left(\frac{p\pi y}{w}\right)\exp(\gamma x). \tag{30b}$$

Hence the embedding potential which replaces this waveguide is given by

$$\Sigma(y, y') = -\frac{1}{w}\sum_p \begin{matrix}\mathrm{i}k_p \\ -\gamma_p\end{matrix}\Bigg\}\sin\left(\frac{p\pi y}{w}\right)\sin\left(\frac{p\pi y'}{w}\right).$$

This gives extra matrix elements to be added onto the Hamiltonian in (7):

$$\int \mathrm{d}y \int \mathrm{d}y'\ \chi_i \Sigma \chi_j \tag{31}$$

with a similar term coming for the right-hand end. The local density of states for the corner connected to the straight waveguide can then be calculated from the Green function for this system:

$$\sigma(\boldsymbol{r}, E) = \frac{1}{\pi} \sum_{ij} \operatorname{Im} G_{ij}(E + \mathrm{i}\epsilon)\chi_i(\boldsymbol{r})\chi_j(\boldsymbol{r}). \tag{32}$$

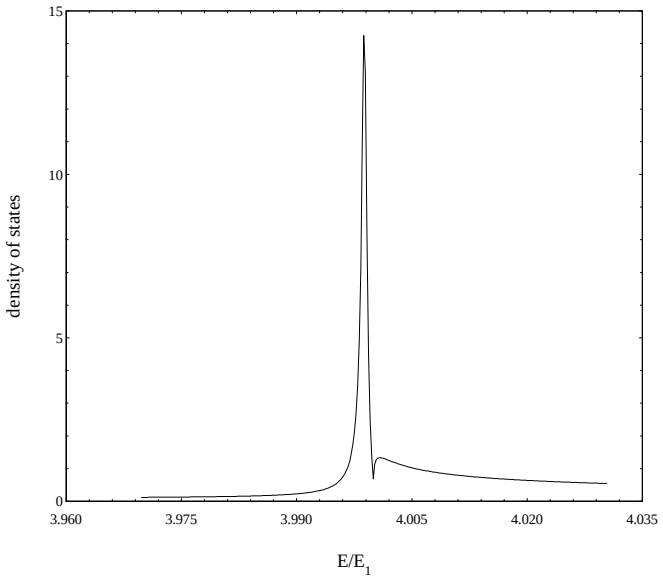

Figure 13. The density of states as a function of the energy (relative to the first threshold energy) for the second threshold energy for the circular corner.

We shall present here the corner density of states $n(E)$, defined as $\sigma(\boldsymbol{r}, E)$ integrated through region I. From (32) this is given simply by

$$n(E) = \frac{1}{\pi} \sum_{ij} \operatorname{Im} G_{ij}(E + \mathrm{i}\epsilon) O_{ij} \tag{33}$$

where O_{ij} is the overlap integral defined in (8).

The density of states for the circular corner is shown in figures 12 and 13. In figure 12 we see the bound state just below the first threshold, at $E = 0.9956E_1$ (it is broadened in figure 12 by a small imaginary part of 0.0002 au added to its energy). An analogous state appears just below the second threshold (figure 13), but this can interact with the continuum and it is broadened—only slightly—into a resonance. The lineshape is characteristic of a Fano resonance [21]. Above the thresholds, E_{th}, the density of states has one-dimensional behaviour, with a contribution varying like $1/(E - E_{th})^{1/2}$ from each open channel [22]. This is modified at thresholds as we see from the figures, rounded off and with the bound state or resonance pulled off. We have seen previously that the transmission round the circular corner is remarkably uniform, apart from anomalies just below thresholds—the anomaly shown in figure 6 is at almost exactly the same energy as the resonance in figure 13, and the two phenomena are presumably linked by scattering theory.

The square corner has a dramatic effect on the density of states (figure 14). Once again, a bound state is pulled off below the first threshold, with a greater binding energy than in

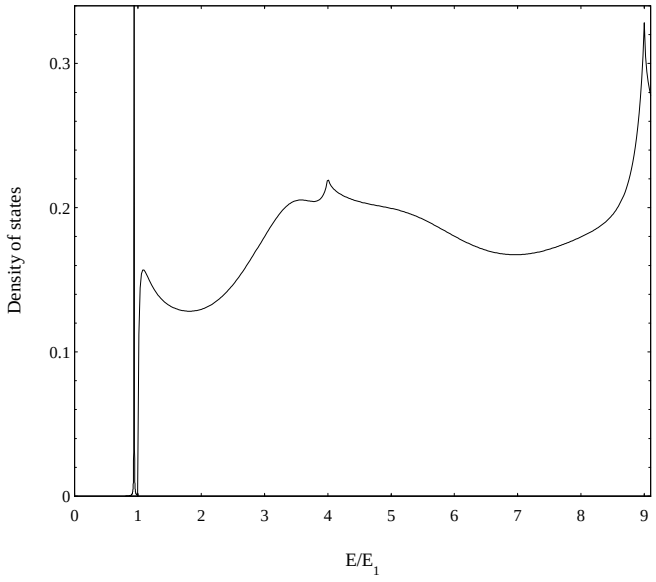

Figure 14. The density of states as a function of the energy (relative to the first threshold energy) for the square corner.

the circular case, $E = 0.9399E_1$. There are no obvious resonances at higher energies—the mixing of channels by the square corner broadens any resonances out completely, but surprisingly enough there are very sharp features at the second and third thresholds. The most striking feature of the density of states of the square corner is how constant it is. It is in fact much more akin to the constant density of states of an (infinite) two-dimensional system than the one-dimensional density of states shown by the circular corner. The density of states in two dimensions is $1/2\pi$ per unit area and with an area of 1.4 included in region I this would give a constant corner density of states of 0.22 au, in fair agreement with figure 14. There is no obvious connection between the rather featureless density of states in this case and the highly structural transmission coefficient. It would be interesting to see whether the densities of states can be explored directly.

6. Conclusion

The embedding method provides a simple and straightforward way to calculate both static and transmission properties of conducting channels, and the flexibility of the basis set will enable other scatterers—such as impurities—to be included in a very simple manner. It also enables us to study the local density of states, on the same footing. We are currently exploring other applications of this method.

Acknowledgments

We thank S V Dewar and J M Heaton for helpful discussions. Support from the EPSRC and a CASE award from DERA, Malvern are gratefully acknowledged.

References

[1] Beenakker C W J and van Houten H 1991 *Solid State Physics* vol 44 (New York: Academic) p 1
[2] Crampin S, Nekovee M and Inglesfield J E 1995 *Phys. Rev.* B **51** 7318
[3] Sols F and Macucci M 1990 *Phys. Rev.* B **41** 11 887
[4] Martorell J, Klarsfeld S, Sprung D W L and Wu Hua 1991 *Solid State Commun.* **78** 13
[5] Wu Hua, Sprung D W L and Martorell J 1992 *J. Appl. Phys.* **72** 151
[6] Berggren K-F and Ji Zhen-Li 1993 *Phys. Rev.* B **47** 6390
[7] Lent C S 1990 *Appl. Phys. Lett.* **56** 2554
[8] Pendry J B, Prêtre A, Rous P J and Martín-Moreno L 1991 *Surf. Sci.* **244** 160
[9] Sheng Wei-Dong 1997 *J. Phys.: Condens. Matter* **9** 8369
[10] Lang N D 1995 *Phys. Rev.* B **52** 5335
[11] Ji Zhen-Li 1992 *Semicond. Sci. Technol.* **7** 198
[12] Ji Zhen-Li 1993 *J. Appl. Phys.* **73** 4468
[13] Berggren K-F, Besev C and Ji Zhen-Li 1992 *Quantum Effect Physics, Electronics and Applications* ed K Ismail, T Ikoma and H I Smith (Bristol: Institute of Physics Publishing) p 25
[14] Lent C S 1990 *Appl. Phys. Lett.* **57** 1678
[15] Tekman E and Bagwell P F 1993 *Phys. Rev.* B **48** 2553
[16] Weisshaar A, Lary J, Goodnick S M and Tripathi V K 1989 *Appl. Phys. Lett.* **55** 2114
[17] Yalabik M C 1994 *IEEE Trans. Electron Devices* **41** 1843
[18] Goldstone J and Jaffe R L 1992 *Phys. Rev.* B **45** 14 100
[19] Price P J 1993 *Appl. Phys. Lett* **62** 289
[20] Ulreich S and Zwerger W 1998 *Europhys. Lett.* **41** 117
[21] Fano U 1961 *Phys. Rev.* **124** 1866
[22] Ferry D K and Goodnick S M 1997 *Transport in Nanostructures* (Cambridge: Cambridge University Press)